(Received 3 September 2023, Accepted 30 November 2023, Scheduled 24 December 2023)

A Novel Pentagonal-Shaped Monopole Antenna with a CSRR Metamaterial Loaded Defected Ground for UWB Applications

Chahrazad Bensid[1], Mohamed Lamine Bouknia[1], Djamel Sayad[2], Issa Elfergani[3,4], Hanane Bendjedi[1], Rami Zegadi[1], Jonathan Rodriguez[3,5], Atul Varshney[6], and Chemseddine Zebiri[1,*]

[1]*Laboratoire d'Electronique de Puissance et Commande Industrielle (LEPCI), Department of Electronics University of Ferhat Abbas, Setif-1-, Setif 19000, Algeria*
[2]*Laboratoire d'Electrotechnique de Skikda (LES), Department of Electrical Engineering University 20 Aout 1955-Skikda, Skikda 21000, Algeria*
[3]*Instituto de Telecomunicações, Campus Universitário de Santiago, 3810-193 Aveiro, Portugal*
[4]*Faculty of Engineering and Informatics, University of Bradford, Bradford BD7 1DP, UK*
[5]*Faculty of Computing, Engineering and Science, University of South Wales, Pontypridd CF37 1DL, UK*
[6]*ECE Department, FET Gurukula Kangri (Deemed to be) University, Haridwar 249404, Uttarakhand, India*

ABSTRACT: This article presents a novel compact ultra-wideband (UWB) planar monopole antenna printed on an FR4 substrate. The antenna consists of a pentagonal radiating element and incorporates loading metamaterial complementary split ring resonator (CSRR) on the ground plane to optimize impedance matching for UWB operation. The overall dimensions of the designed antenna are $17.75 \times 20\,\text{mm}^2$. The proposed compact UWB antenna exhibits an operating bandwidth from 3.01 to 12.41 GHz with a -10 dB return loss and a fractional bandwidth (FBW) of approximately 123%. Additionally, the proposed antenna exhibits a stable radiation pattern with a peak gain of 6.3 dB and a peak radiation efficiency of 98.3%. To validate the simulation results, a prototype has been fabricated and measured, which shows good coherence with the simulation results. In addition, the proposed design is compared with leading antennas for similar applications to demonstrate the suitability of its concept. Moreover, an equivalent circuit model of the CSRR metamaterial cell is developed and validated using ADS software.

1. INTRODUCTION

Monopole antennas have gained widespread importance in day-to-day communication applications due to their small size, low profile, and easy integration into portable devices [1, 2], making them a popular choice for wireless communications. In modern wireless devices like mobile phones and laptops, antennas are usually tuned to specific single-frequency bands of interest. However, with the explosive growth of wireless communication standards, more antennas need to be integrated into devices, increasing complexity; this is where Ultra-Wideband (UWB) technology comes into play.

Nowadays, the UWB technology is very popular in modern wireless communications [1] to meet the requirements of high data rates in short-distance communications, high bandwidth and low power consumption, etc. In 2002, the Federal Communication Commission (FCC) licensed the UWB in the 3.1–10.6 GHz range for commercial applications [3–5]. Since then, it has become extremely popular with researchers. On the other hand, future advances in wireless communication systems and multifunctional devices require the incorporation of UWB technology with a single antenna, one of the main objectives [6].

In parallel with progress in wireless communications, the implementation of a wide bandwidth with sufficient radiation efficiency and the reduction of antenna size in the lowest operational frequency band are the two main objectives in the design of a UWB antenna [7]. Within this framework, numerous geometries have been proposed for UWB applications, such as circular disks [8–10], elliptical disks [11–15], and ring-shaped structures [7, 16, 17]. On the other hand, many researchers have understood that these shapes alone are not sufficient to meet UWB requirements, and various techniques have been harnessed to improve bandwidth. UWB behavior has been achieved via a U-shaped slot in the partial ground plane [18], parasitic elements [19–21], metamaterials [22–25], defected ground structures [26–29], and parasitic slots [30–32]. It is true that there is freedom in choosing the shape of the radiating patch and ground plane structures, but optimizing the overall antenna structure to match the design specifications remains challenging.

In the light of this debate, much remains to be done in terms of miniaturizing the design and improving the impedance bandwidth. Therefore, in this letter, a simple, compact, cost-effective UWB printed monopole antenna is presented. The design and analysis of the antenna are carried out using CST simulator. The simulation is verified by comparing the simulated data with the measured data. The antenna design makes use of a pentagonal radiator fed by a microstrip feedline with an L-shaped defected ground plane. In addition, this letter investigates a simple method of adding parasitic patch elements and loading a complementary split-ring resonator (CSRR) metamaterial in the ground plane. In terms of design structure, this method keeps the profile low. In terms of performance, the

* Corresponding author: Chemseddine Zebiri (czebiri@univ-setfi.dz).

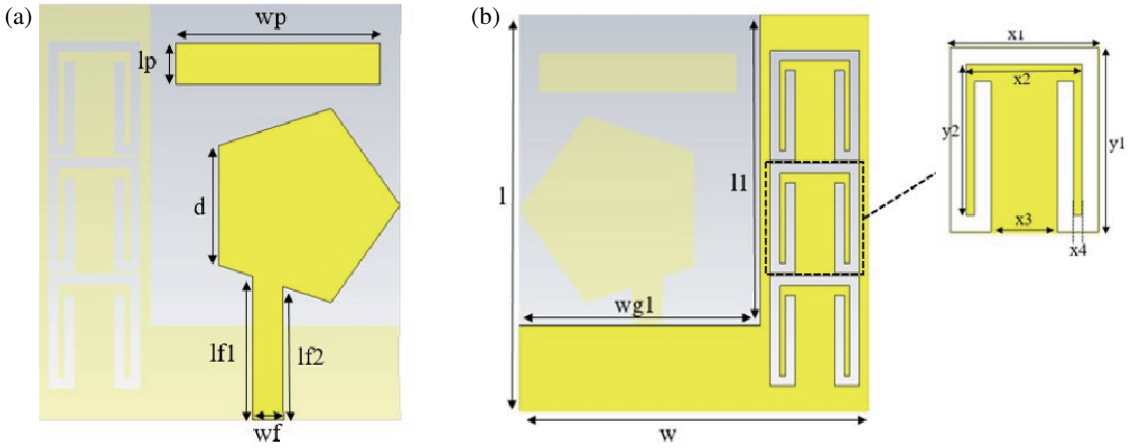

FIGURE 1. Geometry of the proposed UWB antenna, (a): top layout and (b): bottom layout.

TABLE 1. Optimized implantable antenna parameters.

Parameter	**w**	**l**	**wf**	**lf1**	**lf2**	**wp**	**lp**	**D**
Dimension (mm)	17.75	20	1.5	6.9	6.41	10	2	5.76
Parameter	**wg1**	**l1**	**x1**	**x2**	**x3**	**x4**	**y1**	**y2**
Dimension (mm)	12.25	15.5	4.5	3.5	2	0.25	5.5	4.5

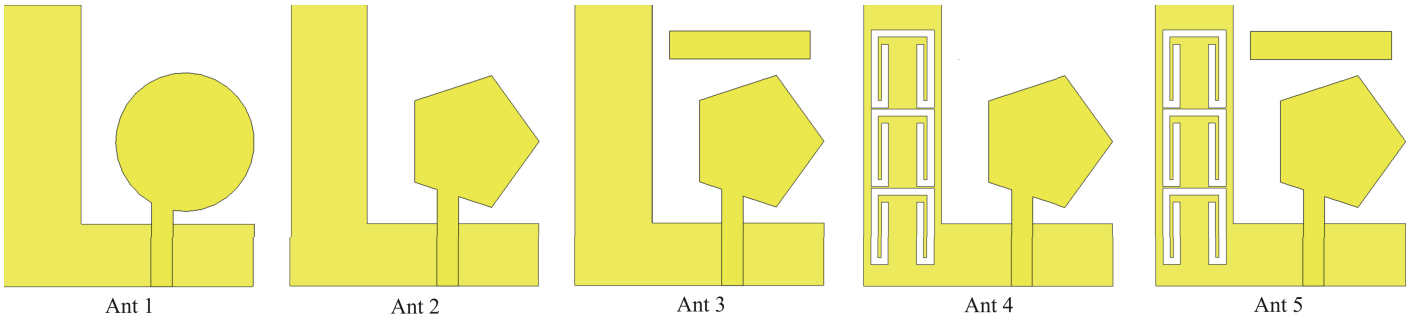

FIGURE 2. Step-by-step design process of the proposed antenna.

antenna's bandwidth is significantly improved, and both efficiency and gain are increased.

2. ANTENNA DESIGN AND CONFIGURATION

2.1. Detailed Dimensions

The proposed antenna (Figure 1) is a microstrip patch antenna printed on an FR-4 substrate with a thickness of $h = 1.6$ mm, a relative dielectric permittivity of $\varepsilon_r = 4.3$, and a loss tangent of 0.0025. To achieve optimal impedance matching, a microstrip feed line is used to excite the antenna. The pentagonal patch antenna has dimensions of $17.75 \times 20\,\text{mm}^2$.

The designed antenna is simulated using Computer Simulation Technology (CST) microwave studio and was tuned to resonate from 3.01 GHz to 12.41 GHz to meet the defined requirements. The different geometrical parameters of this antenna are shown in Figure 1, and all the parameters used to design this antenna are listed in Table 1.

2.2. Design Procedures of the Proposed UWB Antenna

In this section, we present a comprehensive description of the step-by-step implementation of the proposed UWB antenna. We start by providing a detailed account of the construction process, outlining the required materials and components. Subsequently, we delve into the operating procedures, offering an in-depth explanation of how the antenna functions and interacts within its environment.

The proposed antenna has been evaluated in terms of reflection coefficient, gain, and efficiency with different scenarios (Figure 2).

Simulation studies of the proposed antenna are carried out using CST, and the results are discussed in the following sections. The simulated results are presented in Figure 3, which shows the various response parameters for different scenarios. Table 2 summarizes the performance characteristics of the antenna scenarios obtained in Figure 3. Initially, a monopole antenna is proposed with a circular patch and a modified L-shaped

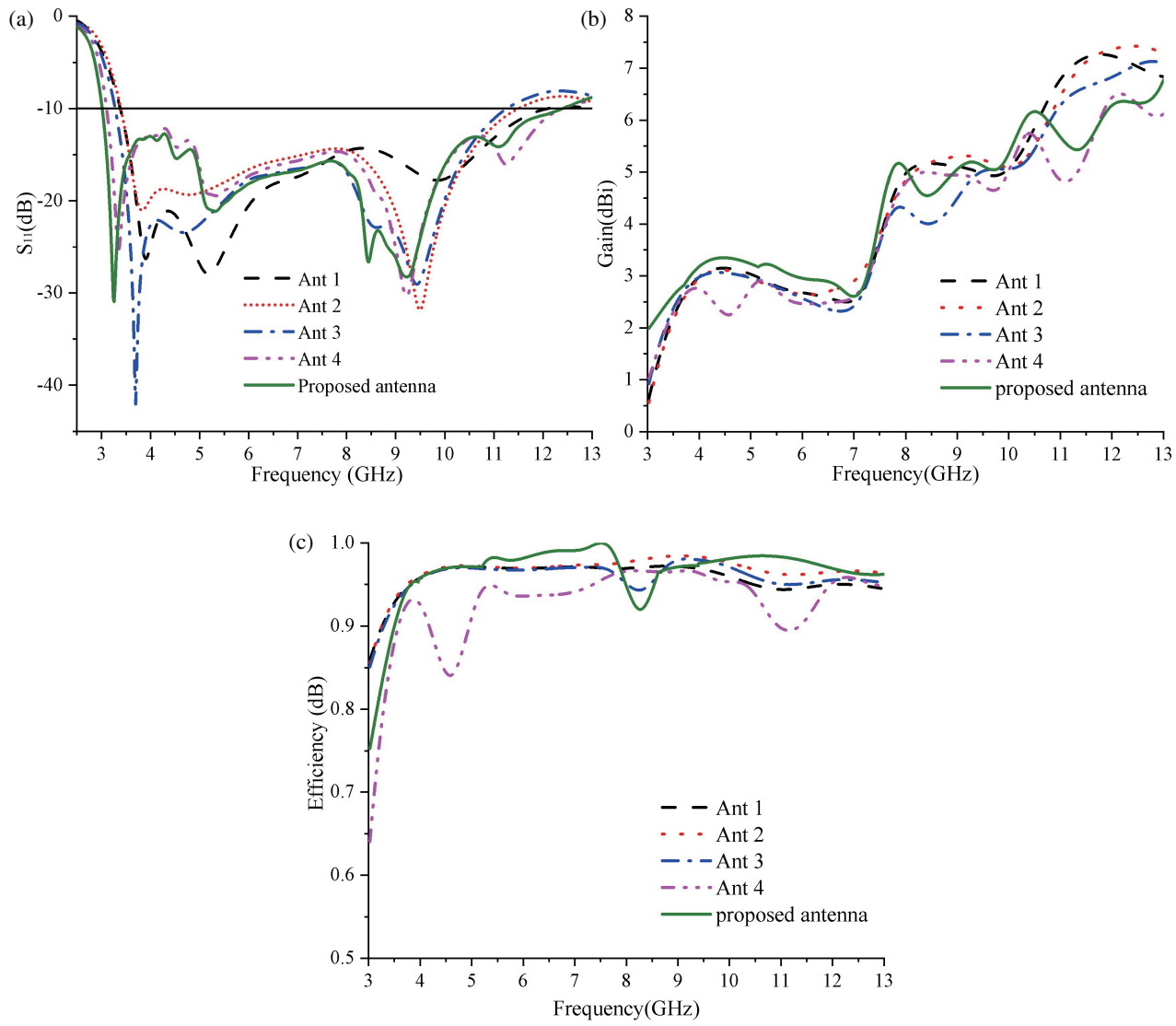

FIGURE 3. Results of the different design stages (a) S_{11}, (b) Gain and (c) Efficiency.

ground plane as shown in Figure 2 (Ant 1). The model in this scenario operates in the 3.45–11.48 GHz band. To improve the bandwidth of this antenna, we change the shape of the radiating element into a pentagonal shape as shown in Figure 2 (Ant 2), which enhances the antenna bandwidth to cover the band from 3.4 to 12.1 GHz. However, it does not cover the lower UWB frequencies as indicated by the FCC. No significant changes in gain and efficiency performance compared to the first scenario are observed. On the other hand, a thorough investigation of the influence of the parasitic element and CSRR metamaterial on the antenna's performance is conducted in scenarios 3 and 4, respectively.

The introduction of the parasitic element improves the bandwidth characteristics (Ant 3). The operating band has been extended from 3.28 to 11.25 GHz, yet still fails to meet the FCC requirements. By loading the CSRR metamaterial (Ant 4) on the ground plane, a significant increase in the operating band is observed with a decrease in gain and efficiency. The proposed antenna is a combination of scenarios 2, 3, and 4. A significant change is observed in the antenna operating band, which meets the UWB band requirements by covering the entire ultra-wideband frequency from 3.01 to 12.41 GHz and improving both gain and efficiency.

Figure 4 depicts the simulated radiation pattern of the step-by-step implementation of the proposed UWB antenna. The results indicate that the antenna offers stable radiation patterns in the covered frequency band.

Figure 5 compares the axial ratio of the antenna at different design stages. The circular and pentagonal patch structures (Ant 1 and Ant 2) exhibit linear polarization characteristics. The introduction of the parasitic element increases the antenna current path, resulting in a circular polarization characteristic. The axial ratio is reduced to 3 dB at 8 GHz. Therefore, the circular polarization characteristics are achieved by introducing the parasitic element.

In order to characterize the effect of the CSRR metamaterial structure, the proposed CSRR unit cell CST simulation setup is shown in Figure 6(a). The unit cell is placed between two

TABLE 2. Performance comparison of UWB antenna.

Design	Band (GHz)	Bandwidth (%)	Gain range (dB)	Efficiency (%)	Axial ratio (dB)
Ant 1	3.45–11.48	107%	0.63–5.65	94%	12–28
Ant 2	3.4–12.1	112%	0.5–5.4	95.6%	11.7–23
Ant 3	3.28–11.25	109%	0.84–5.2	94.8%	2.7–32.6
Ant 4	3.15–12.4	117%	1.1–5.52	92.7%	8.4–34
Ant 5	3.01–12.41	123%	2–6.3	98.3%	2.9–35

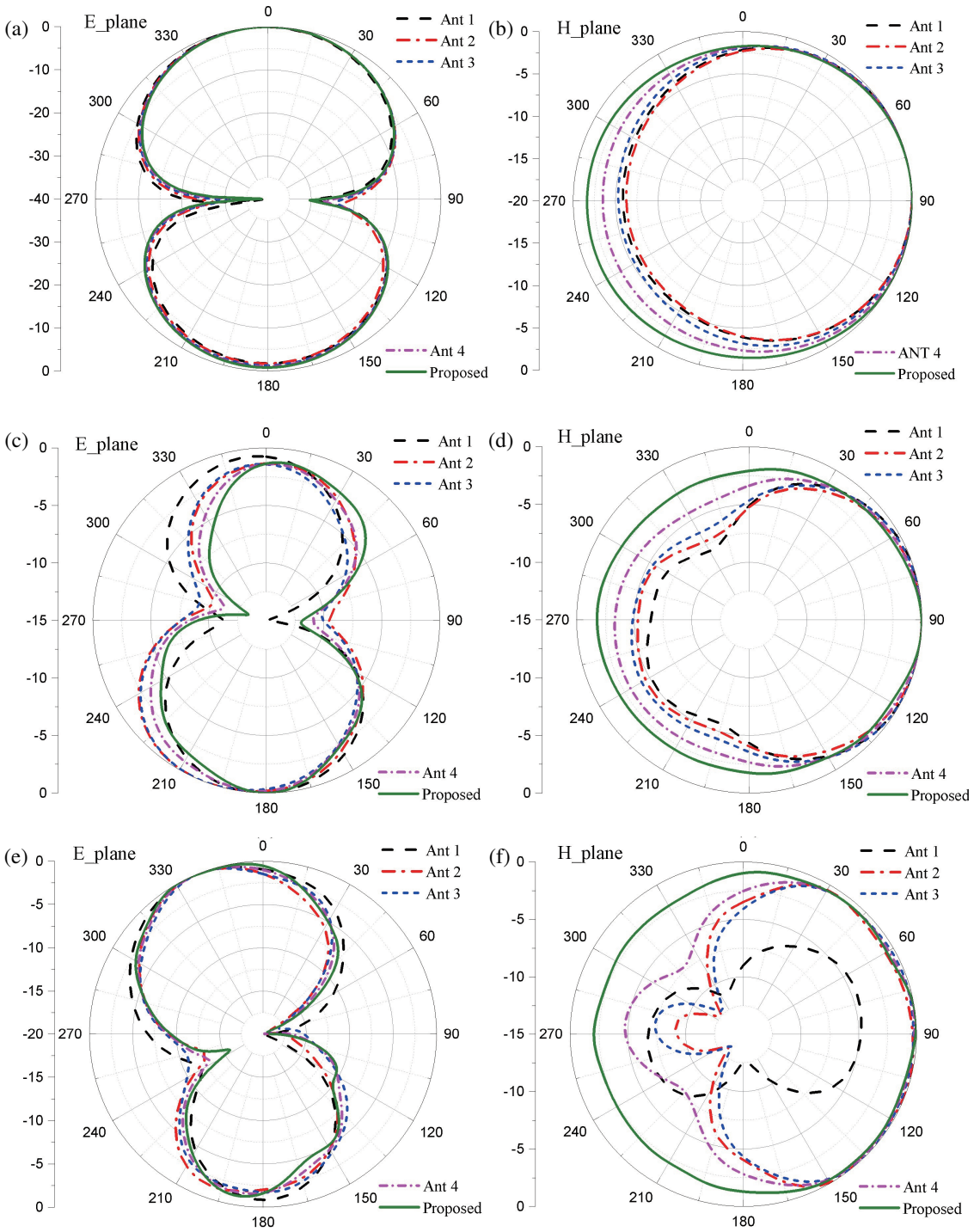

FIGURE 4. Radiation pattern of the different design steps (a), (b) 3.55 GHz, (c), (d) 7.75 GHz and (e), (f) 10.6 GHz.

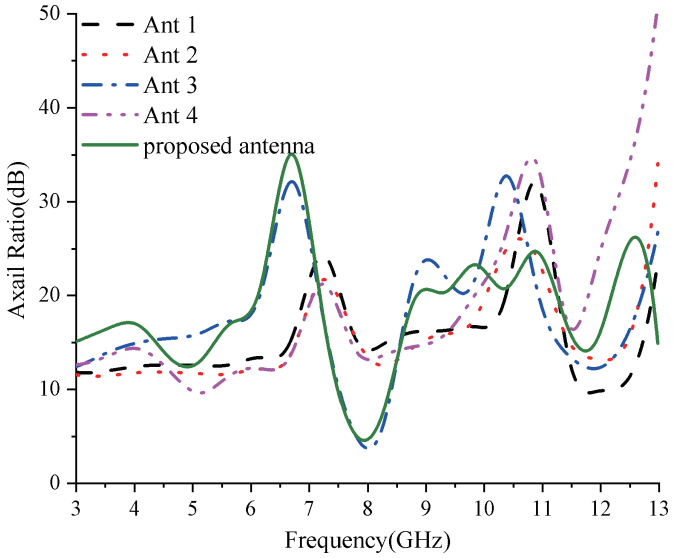

FIGURE 5. Axial ratio of the different design steps.

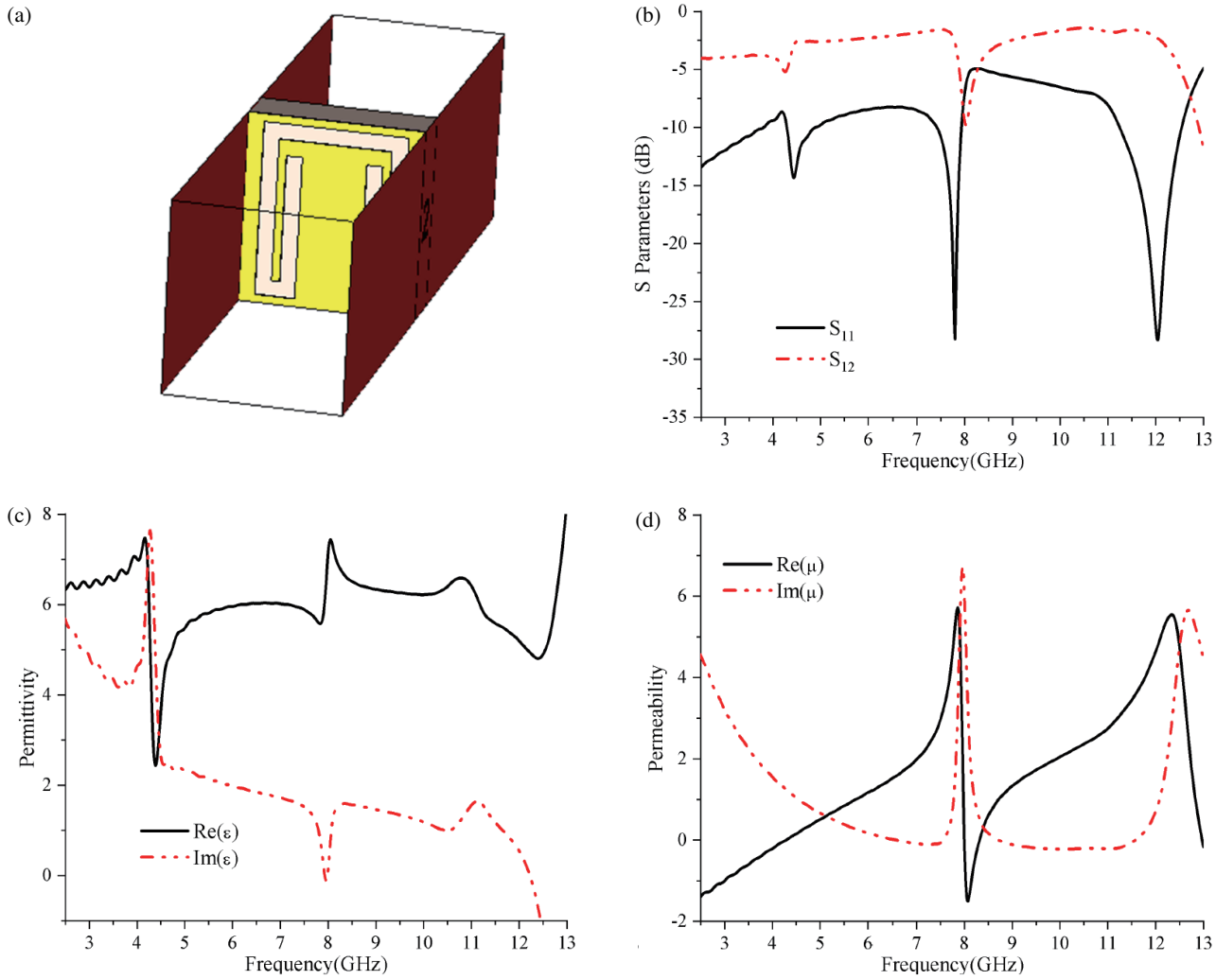

FIGURE 6. CSRR unit cell characteristics. (a) Simulation setup. (b) S-parameters. (c) Permittivity. (d) Permeability.

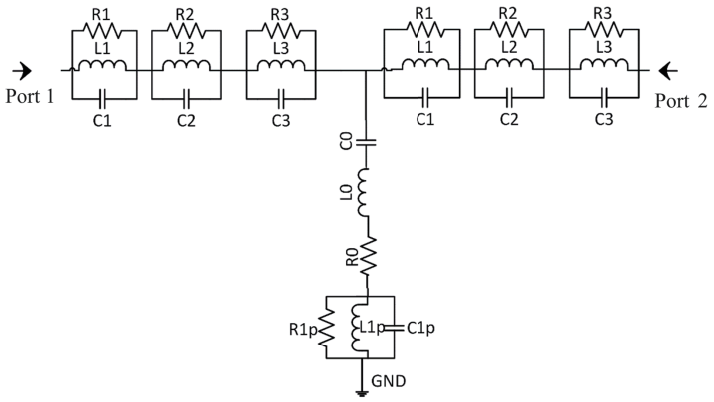

FIGURE 7. Equivalent circuit model of CSRR unit cell.

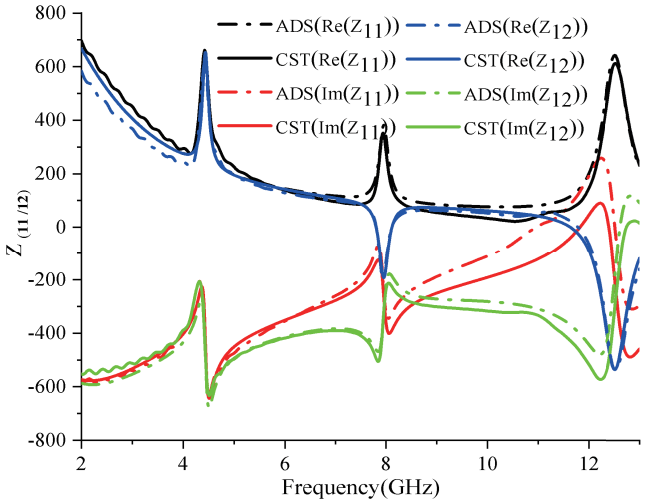

FIGURE 8. ADS and CST simulated Z parameters.

waveguide ports located along the negative and positive z-axis. In analyzing the features of the proposed metamaterial structure for incorporation in the antenna design, the reflection (S_{11}) and transmission (S_{21}) coefficients are extracted to compute the effective permittivity (ε_r) and permeability (μ_r), expressed as follows [33].

$$v_1 = s_{21} + s_{11} \tag{1}$$

$$v_2 = s_{21} - s_{11} \tag{2}$$

$$\text{Effective Permittivity, } \varepsilon_r = \frac{2}{jk_0 d}\frac{1 - v_1}{1 + v_1} \tag{3}$$

$$\text{Effective Permeability, } \mu_r = \frac{2}{jk_0 d}\frac{1 - v_2}{1 + v_2} \tag{4}$$

where $k_0 = \frac{\omega}{c} = \frac{2\pi f}{c}$ and d is the slab thickness.

The metamaterial's electromagnetic characteristics can be described by the coefficients of the S parameters (S_{11} and S_{21}). Figure 6(b) shows the result of the reflectance resonance (S_{11}) of the dual-band C-SRR at 4.8 and 11.35 GHz (amplitude of -26 dB and -16 dB, respectively) and the transmittance (S_{21}) at 7.29 GHz (amplitude of -41 dB). The effective permittivity and permeability of the integrated C-SRR metamaterial structure are illustrated in Figures 6(c) and (d), where negative permittivity is achieved in two frequency ranges. The first is roughly between 2 and 4.4 GHz, while the second is between 5.1 and 7.42 GHz. In addition, negative permeability is achieved between 7.5 and 13 GHz. It can be seen that dual-band C-SRR behaves as negative permittivity (ENG) at 4.8 GHz and negative permeability (MNG) at 11.35 GHz.

The equivalent circuit model of the designed CRSS metamaterial cell is shown in Figure 7. In the circuit model, the combination of inductors and capacitors is both in series and in parallel.

The metamaterial cell of Figure 6(a) can be electromagnetically described through the S parameters (Figure 6(b)). The CSRR's S_{11} parameter results show three peaks of -15, -28 and -27 dB observed at resonance frequencies around 4, 8, and 12 GHz, respectively. The S_{21} shows a peak of -11.4 dB at 8.07 GHz. The effective permittivity and permeability of the CSRR metamaterial structure are illustrated in Figure 6(c) and (d), where a negative permeability is achieved in 2–4.3 GHz and 7.8–8.12 GHz frequency bands. In addition, the permittivity is positive over the frequency band. The CSRR cell consists of a slot, a rectangular patch, and a PI-shaped resonator. The equivalent circuit model of the proposed CSRR metamaterial cell is shown in Figure 7. Combinations of resistors, inductors, and capacitors in series and parallel circuits are used to model the CSRR cell based on the transmission line and resonator models, where the line and resonator are represented by the series and parallel RLC circuits, respectively [34–36]. The T-shaped equivalent electrical circuit of the proposed CSRR cell is represented by three resonator circuits and a microstrip transmission line with a resonator as a coupling part. The slot, rectangular patch, and PI-shaped resonator behave like three RLC parallel circuits defined by resistance (R1, R2, and R3), inductance (L1, L2, and L3), and capacitance (C1, C2, and C3). The coupling part is modelled by R0, L0, C0 series circuit and R1p, L1p, C1p parallel circuit representing the transmission line and rectangular patch in direct contact with the two ports. The RLC (R0, L0, C0) series and (R1p, L1p, C1p) parallel circuits are the microstrip line and the rectangular-shaped resonator, respectively. To verify the accuracy of the proposed electrical equivalent circuit model, its impedance matrix elements, extracted using ADS software, are compared to the CST simulations. As illustrated in Figure 8, the real and imaginary parts of both Z11 and Z12 parameters exhibit remarkable agreement, confirming the validity of the proposed circuit.

3. RESULTS AND DISCUSSION

To support the proposed concept and the simulation results, a prototype antenna is fabricated and measured.

Figure 9 shows photographs of the fabricated UWB-CSRR-loaded defected ground pentagonal-shaped monopole antenna based on the above-mentioned parameters. The return loss,

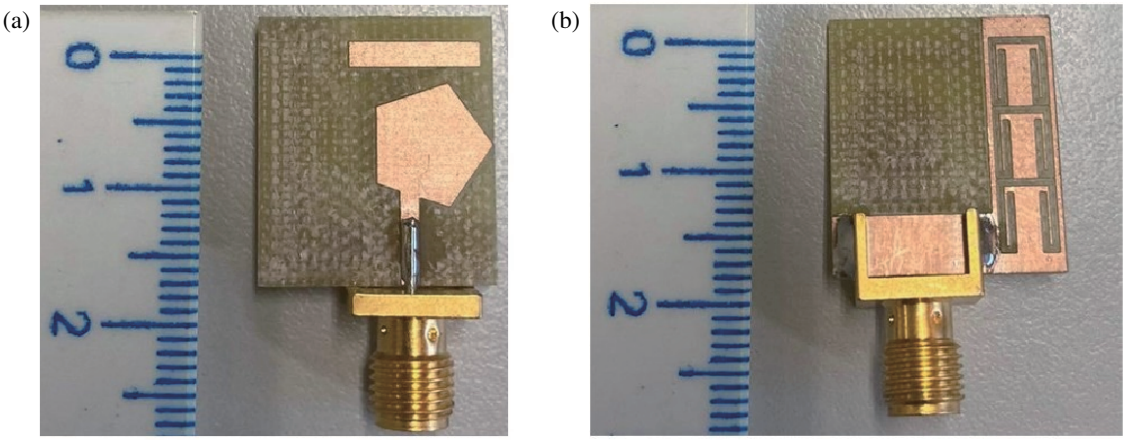

FIGURE 9. Fabricated prototype of the proposed UWB antenna (a) top (b) bottom view.

TABLE 3. Performance comparison of the proposed antenna.

Ref	Year	Overall size (mm)	Freq. (GHz)	Impedance bandwidth %	Peak Gain (dB)	Efficiency (%)
[6]	2019	30 × 25 × 0.8	3.1–11.5	114	5.25	NR
[10]	2021	38 × 48 × 1.6	2.33–14.3	143	8.4	NR
[12]	2020	25 × 25 × 1.45	3.1–16.243	136	4.56	NR
[20]	2022	24 × 28	2.9–11.75	120	5.7	92.3
[26]	2020	25 × 26 × 1.6	3.10–10.9	114	3.8	NR
[27]	2019	17 × 22 × 1.588	2.9–11.4	118	>2	88.5
[28]	2022	30 × 17.59 × 1.6	2.66–10.80	119	3.38	99.96
[7]	2023	15 × 20 × 1.6	3.1–18.1	141.51	5.4	90
[31]	2023	24 × 28 × 1.6	3.42–11.79	110	4.08	NR
[33]	2023	30 × 35 × 1.6	3.5–10.4	99.28	NR	NR
Proposed antenna		17.75 × 120 × 11.6	3.01–12.41	123	6.3	98.3

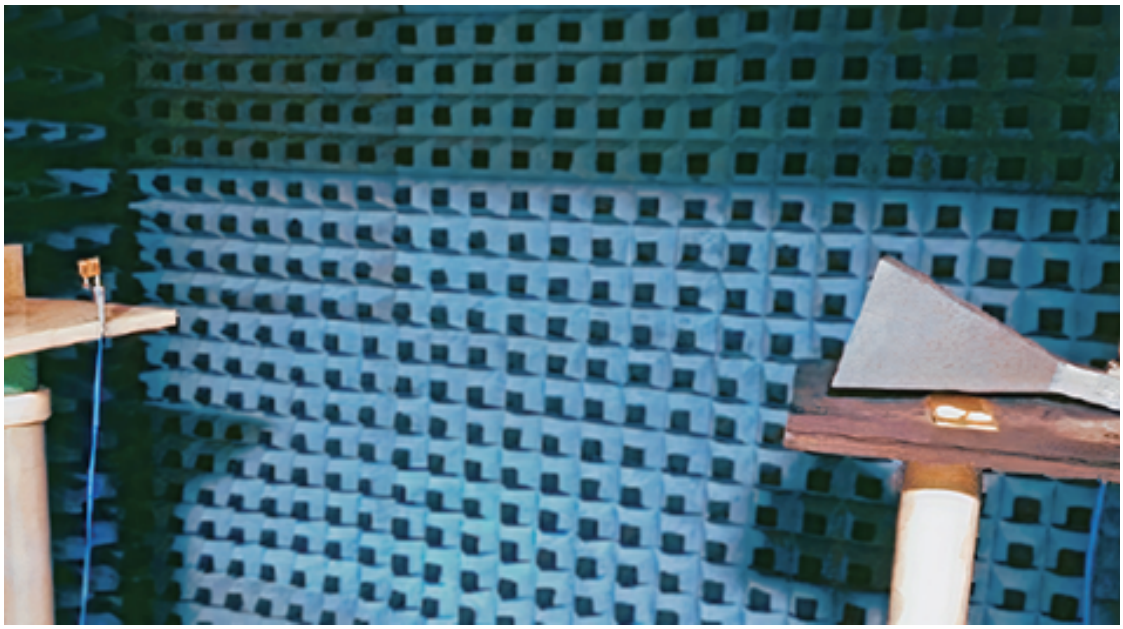

FIGURE 10. Radiation pattern measurement setup inside an anechoic chamber.

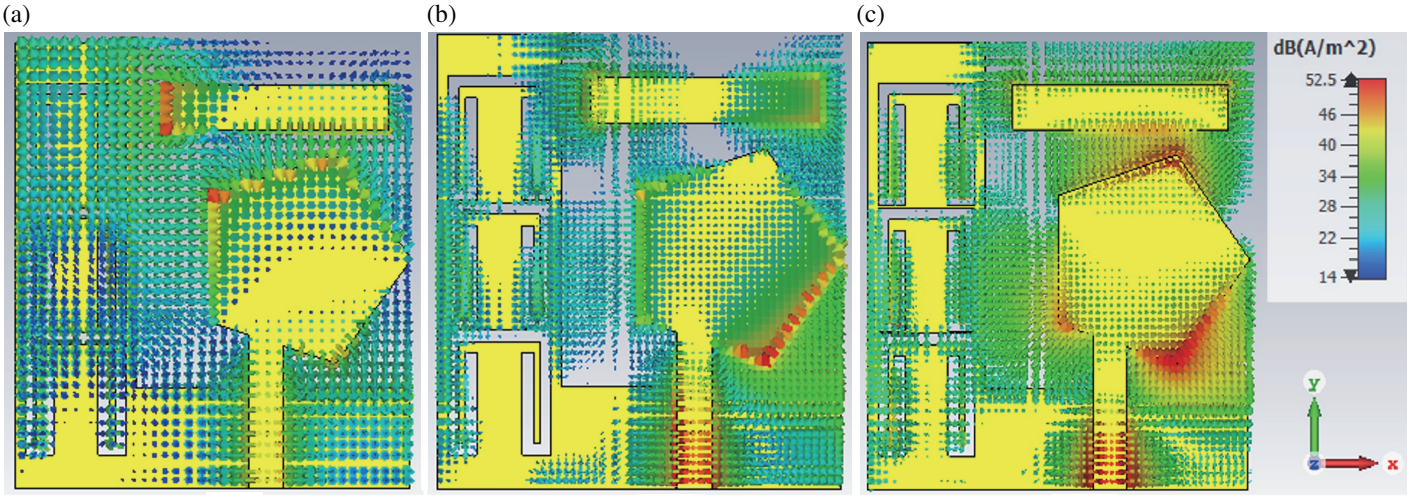

FIGURE 11. Current distributions at (a) 3.1 GHz, (b) 7.75 GHz and (c) 10.6 GHz.

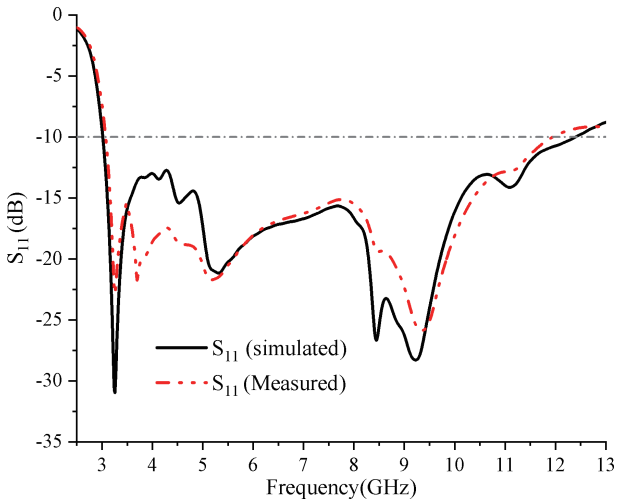

FIGURE 12. Simulated and measured S_{11} of the proposed antenna.

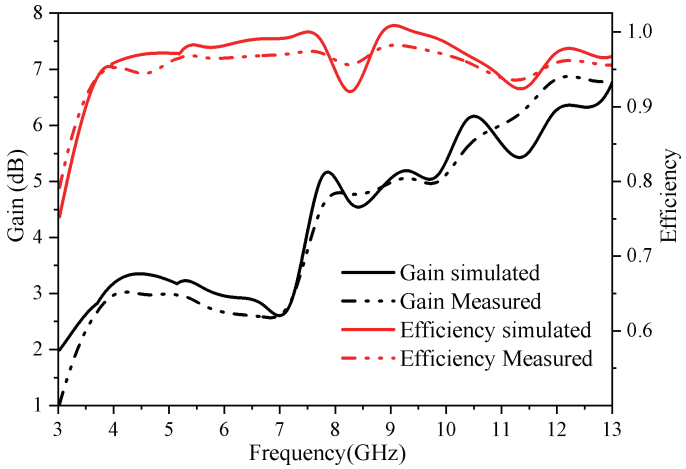

FIGURE 13. Simulated and measured gain and efficiency.

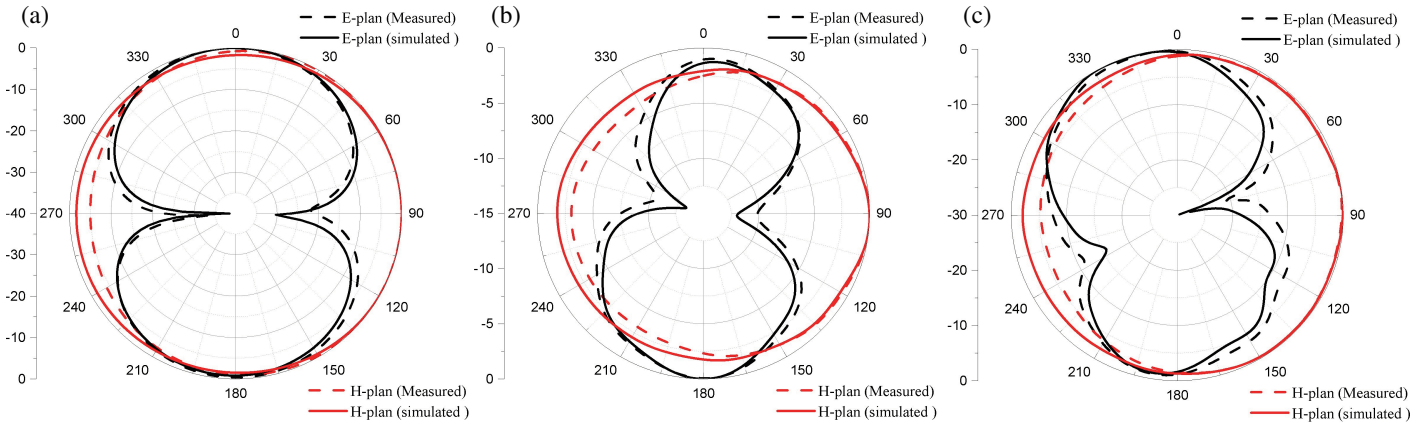

FIGURE 14. Simulated and measured radiation patterns at (a) 3.1 GHz, (b) 7.75 GHz and (c) 10.6 GHz.

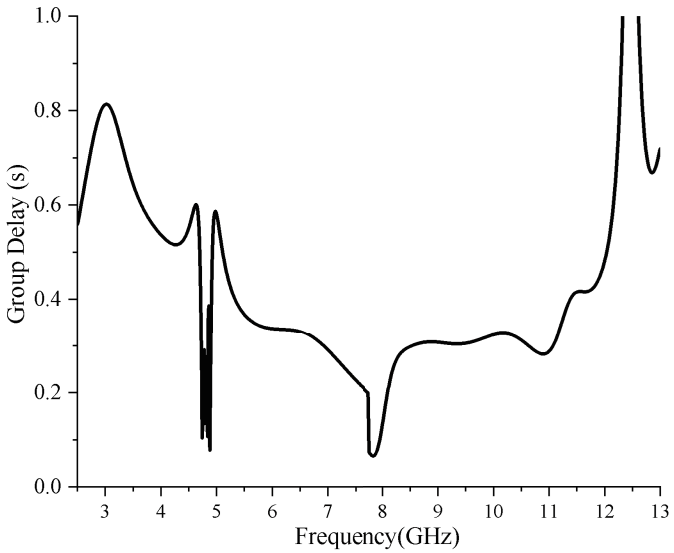

FIGURE 15. Simulated group delay of the proposed antenna.

gain, efficiency, and radiation pattern of the proposed antenna are then measured.

To conduct the S-parameters measurements, the design prototype is connected to the performance network analyzer PNA-X Vector Network Analyzer in a free space environment. Each antenna is connected to the PNA port by a low loss 50 Ω feed cable. Figure 10 shows the radiation pattern measurements setup inside an anechoic chamber. A horn antenna is used as a transmitter and the design under test as a receiver. Both antennas are connected to the VNA, which provides the necessary power to the horn and collects the measured data from the AUT.

To better understand the radiating behavior of the proposed antenna, Figure 11 demonstrates the surface current distributions describing the radiation mechanism at different operating frequencies. The first observation that we extrapolate from the picture is the spread of the current density on the edges of the structure for all frequencies, and it is not located in the center of the pentagonal patch, which enhances the radiation process. Figure 11(a) shows a maximum current density around the upper part, between the parasitic element and the CSRR, which results in the generation of the lower resonance frequency (3.1 GHz). The current is distributed across the feed line and the pentagonal radiator lower side (Figure 11(b)) and all its sides and the feed (Figure 11(c)), which causes the generation of higher resonances at 7.75 GHz and 10.6 GHz, respectively.

3.1. Experimental Validation

The simulated and measured S_{11} parameters of the proposed antenna are shown and compared in Figure 12. In general, good agreement is observed, and both simulated and measured results satisfy the bandwidth requirements. However, some mismatch between simulations and experiments is observed within the 3.5–5 GHz and 8 GHz frequency bands which corresponds to the regions of the CSRR's metamaterial frequency response (activity) as supported by Figure 6. This may be attributed to experimental inaccuracies on one hand and simulation assumptions on the other hand. However, this mismatch is bound and lies within admissible margins.

Figure 13 shows the gain and efficiency of the proposed UWB antenna. The measured gain varies between 2 and 6.3 dBi in the operating frequency band and tends to increase with frequency. The efficiency fluctuates between 80% and 98% in the operating band, and good agreement is achieved with measurements.

The radiation pattern of the proposed UWB antenna is shown in Figure 14. In the E-plane, the antenna exhibits a dipole-like bidirectional radiation pattern at 3.1 GHz, while slightly right- and left-handed bidirectional radiation patterns are observed at 7.75 GHz and 10.6 GHz, respectively. On the other hand, the antenna exhibits an almost omnidirectional radiation pattern in the major H-plane at resonant frequencies 3.1 GHz, 7.75 GHz, and 10.6 GHz. In general, there is a strong agreement between simulated and measured results for different frequencies. The group delay of the UWB antenna is set up by positioning two UWB antennas almost 6 times the wavelength of the lowest operating frequency (60 cm) from each other in the face-to-face orientation [37]. Figure 15 indicates that the variation in the group delay time is minimal and less than 0.8 ns. Therefore, this antenna has the ability to send and receive short pulse signals without distortion [37, 38].

Table 3 summarizes the performances of the proposed UWB antenna compared with related recently published works. The proposed UWB antenna surpasses all related works in terms of compact size, wide bandwidth, comparable peak gain, efficiency, and low configuration complexity.

4. CONCLUSION

This article presents a new compact monopole antenna for UWB applications. The proposed antenna consists of a pentagonal radiator with a parasitic patch element and an L-shaped CSRR-loaded defected ground plane. The design exhibits an impedance bandwidth of 123% (3.01–12.41 GHz). A proto-

type is manufactured and tested as a proof of concept. The proposed monopole antenna achieved its high gain by carefully optimizing the antenna geometry and dimensions compared with other designs for applications in the same frequency band. A peak gain of 6.3 dB and a peak radiation efficiency of 98% were achieved with a very compact overall volume of $17.75 \times 20 \times 1.6\,\text{mm}^3$. The proposed antenna is a promising candidate for a wide range of UWB applications. The compact size and high performance make it suitable for integration into portable and wearable devices. For further understanding the metamaterial behavior, an equivalent circuit has been presented, discussed, and validated versus extracted ADS Z matrix.

ACKNOWLEDGEMENT

This work was supported in part by the DGRSDT (Direction Générale de la Recherche Scientifique et du Développement Technologique), MESRS (Ministry of Higher Education and Scientific Research), Algeria. Also, is supported in part by the European Union's Horizon 2020 Research and Innovation Program under Grant H2020-MSCA-RISE-2018-EXPLOR-872897, in part by the Fundação para a Ciência e a Tecnologia (FCT)/MEC through national funds and when applicable co-financed by the European Regional Development Fund (ERDF) under Grant PT2020, and in part by the Partnership Agreement under Project UID/EEA/50008/2020.

REFERENCES

[1] Baudha, S. and M. V. Yadav, "A compact ultra-wide band planar antenna with corrugated ladder ground plane for multiple applications," *Microwave and Optical Technology Letters*, Vol. 61, No. 5, 1341–1348, May 2019.

[2] Pandhare, R. A., M. P. Abegaonkar, and C. Dhote, "High gain frequency reconfigurable multifunctional antenna for modern wireless and mobile communication systems," *International Journal of RF and Microwave Computer-aided Engineering*, Vol. 32, No. 11, Nov. 2022.

[3] Zhang, R., Y. C. Liang, P. S. P. Hall, P. Gardner, J. Kelly, E. Ebrahimi *et al.*, "Federal communications commission revision of part 15 of the commission's rules regarding ultra-wideband transmission systems," *FCC, Washington, Dc, First Report & Order*, Vol. 48, No. 1, 133–135, 2009.

[4] Zebiri, C., D. Sayad, I. T. E. Elfergani, J. S. Kosha, W. F. A. Mshwat, C. H. See, M. Lashab, J. Rodriguez, K. H. Sayidmarie, H. A. Obeidat, and R. A. Abd-Alhameed, "Antenna for ultra-wideband applications with non-uniform defected ground plane and offset aperture-coupled cylindrical dielectric resonators," *IEEE Access*, Vol. 7, 166 776–166 787, 2019.

[5] Mohandoss, S., R. R. Thipparaju, B. N. B. Reddy, S. K. Palaniswamy, and P. Marudappa, "Fractal based ultra-wideband antenna development for wireless personal area communication applications," *AEU-International Journal of Electronics and Communications*, Vol. 93, 95–102, 2018.

[6] Nadh, B. P., B. T. P. Madhav, M. S. Kumar, M. V. Rao, and T. Anilkumar, "Circular ring structured ultra-wideband antenna for wearable applications," *International Journal of RF and Microwave Computer-aided Engineering*, Vol. 29, No. 4, Apr. 2019.

[7] Sayad, D., C. Zebiri, H. Obeidat, I. Elfergani, A. Amroun, M. Palandoken, M. LBouknia, R. Zegadi, and J. Rodriguez, "New elliptical miniaturized antenna using concentric open rings for UWB applications," *Progress In Electromagnetics Research C*, Vol. 134, 79–91, 2023.

[8] Yadav, M. V. and S. Baudha, "A compact mace shaped ground plane modified circular patch antenna for ultra-wideband applications," *Telecommunications and Radio Engineering*, Vol. 79, No. 5, 2020.

[9] Tan, W., X. Shan, and Z. Shen, "Ultrawideband circularly polarized antenna with shared semicircular patches," *IEEE Transactions on Antennas and Propagation*, Vol. 69, No. 6, 3555–3559, Jun. 2021.

[10] Gopi, D., A. R. Vadaboyina, and J. R. K. K. Dabbakuti, "DGS based monopole circular-shaped patch antenna for UWB applications," *SN Applied Sciences*, Vol. 3, No. 2, Jan. 2021.

[11] Singhal, S., "Ultrawideband elliptical microstrip antenna for terahertz applications," *Microwave and Optical Technology Letters*, Vol. 61, No. 10, 2366–2373, Oct. 2019.

[12] Majeed, A. H. and K. H. Sayidmarie, "Flower shaped elliptical patch antenna for UWB applications," *International Journal of Microwave and Optical Technology*, Vol. 15, No. 2, 168–178, 2020.

[13] Jose, J., A. S. R. Paulson, and M. J. Jose, "Double-elliptical shaped miniaturized micro strip patch antenna for ultra-wide band applications," *Progress In Electromagnetics Research C*, Vol. 97, 95–107, 2019.

[14] Saeidi, T., I. Ismail, W. P. Wen, and A. R. H. Alhawari, "Ultra-wideband elliptical patch antenna for microwave imaging of wood," *International Journal of Microwave and Wireless Technologies*, Vol. 11, No. 9, 948–966, Nov. 2019.

[15] Alani, S., Z. Zakaria, and A. Ahmad, "Miniaturized UWB elliptical patch antenna for skin cancer diagnosis imaging," *International Journal of Electrical & Computer Engineering (2088-8708)*, Vol. 10, No. 2, 2020.

[16] Gupta, M., K. K. Mutai, V. Mathur, and D. Bhatnaga, "A novel elliptical ring microstrip patch antenna for ultra-wideband applications," *Wireless Personal Communications*, Vol. 114, No. 4, 3017–3029, Oct. 2020.

[17] Amroun, A., C. Zebiri, D. Sayad, I. T. E. Elfergani, A. Desai, M. L. Bouknia, R. Zegadi, and J. Rodriguez, "Miniaturized six-ring elliptical monopole-based mimo antenna for ultrawideband applications," *International Journal of Communication Systems*, Vol. 36, No. 14, Sep. 2023.

[18] Ghimire, J. and D.-Y. Choi, "Design of a compact ultrawideband U-shaped slot etched on a circular patch antenna with notch band characteristics for ultrawideband applications," *International Journal of Antennas and Propagation*, Vol. 2019, 2019.

[19] Alam, M. M., R. Azim, N. M. Sobahi, A. I. Khan, and M. T. Islam, "An asymmetric CPW-fed modified bow tie-shaped antenna with parasitic elements for ultra-wideband applications," *International Journal of Communication Systems*, Vol. 35, No. 9, Jun. 2022.

[20] Venkata, S. G. and S. R. Kalva, "A novel UWB antenna with dual band notched characteristics using a single parasitic," *Progress In Electromagnetics Research C*, Vol. 125, 83–92, 2022.

[21] Babu, K. V., S. Das, G. N. J. Sree, S. K. Patel, M. P. Saradhi, and M. R. N. Tagore, "Design and development of miniaturized MIMO antenna using parasitic elements and machine learning (ML) technique for lower sub 6 GHz 5G applications," *Aeu-international Journal of Electronics and Communications*, Vol. 153, Aug. 2022.

[22] Bouknia, M. L., C. Zebiri, D. Sayad, I. Elfergani, S. Mosbah, J. Rodriguez, and R. A. Abd-Alhameed, "A new compact printed monopole antenna based on compressed metamaterials for UWB applications," in *2021 IEEE 26th International Workshop on Computer Aided Modeling and Design of Communication Links and Networks (CAMAD)*, Electr Network, Oct 25-27, Oct. 2021.

[23] Ali, W. A. E., H. A. Mohamed, A. A. Ibrahim, and M. Z. M. Hamdalla, "Gain improvement of tunable band-notched UWB antenna using metamaterial lens for high speed wireless communications," *Microsystem Technologies-micro-and Nanosystems-information Storage and Processing Systems*, Vol. 25, No. 11, 4111–4117, Nov. 2019.

[24] Fertas, K., F. Ghanem, A. Azrar, and R. Aksas, "UWB antenna with sweeping dual notch based on metamaterial SRR fictive rotation," *Microwave and Optical Technology Letters*, Vol. 62, No. 2, 956–963, Feb. 2020.

[25] Parameswari, S. and C. Chitra, "Textile UWB antenna with metamaterial for healthcare monitoring," *International Journal of Antennas and Propagation*, Vol. 2021, Dec. 2021.

[26] Jan, N. A., S. H. Kiani, F. Muhammad, D. A. Sehrai, A. Iqbal, M. Tufail, and S. Kim, "V-shaped monopole antenna with chichena itzia inspired defected ground structure for UWB applications," *CMC-computers Materials & Continua*, Vol. 65, No. 1, 19–32, 2020.

[27] Venkatachalam, D. and M. Govindasamy, "A miniaturized planar antenna with defective ground structure for UWB applications," *IEICE Electronics Express*, Vol. 16, No. 14, Jul. 2019.

[28] Ibnyaich, S., S. Chabaa, L. Wakrim, A. E. Yassini, A. Zeroual, and M. M. Hassani, "A pentagonal shaped microstrip planar antenna with defected ground structure for ultrawideband applications," *Wireless Personal Communications*, Vol. 124, No. 1, 499–515, May 2022.

[29] Babu, K. V. and B. Anuradha, "Design of MIMO antenna to interference inherent for ultra wide band systems using defected ground structure," *Microwave and Optical Technology Letters*, Vol. 61, No. 12, 2698–2708, Dec. 2019.

[30] Hassan, M. M., M. Rasool, M. U. Asghar, Z. Zahid, A. A. Khan, I. Rashid, A. Rauf, and F. A. Bhatti, "A novel UWB MIMO antenna array with band notch characteristics using parasitic decoupler," *Journal of Electromagnetic Waves and Applications*, Vol. 34, No. 9, SI, 1225–1238, Jun. 2020.

[31] Devana, V. N. K. R. and A. M. Rao, "Design and analysis of dual band-notched UWB antenna using a slot in feed and asymmetrical parasitic stub," *IETE Journal of Research*, Vol. 69, No. 1, 284–294, Jan. 2023.

[32] Babu, K. J., R. W. Aldhaheri, L. S. Sai, B. R. Perli, T. Addepalli, S. R. Pasumarthi, B. K. Kumar, and V. N. K. R. Devana, "Design and modal analysis of dual-slot circular patch antenna for ultra-wideband applications," *Journal of Optoelectronics and Advanced Materials*, Vol. 24, No. 7-8, 355–364, Jul-aug. 2022.

[33] Mahmud, M. Z., M. T. Islam, N. Misran, M. J. Singh, and K. Mat, "A negative index metamaterial to enhance the performance of miniaturized UWB antenna for microwave imaging applications," *Applied Sciences-basel*, Vol. 7, No. 11, Nov. 2017.

[34] Almutairi, A. F., M. S. Islam, M. Samsuzzaman, M. T. Islam, N. Misran, and M. T. Islam, "A complementary split ring resonator based metamaterial with effective medium ratio for C-band microwave applications," *Results in Physics*, Vol. 15, Dec. 2019.

[35] Abdulkarim, Y. I., L. Deng, M. Karaaslan, S. Dalgac, R. H. Mahmud, F. O. Alkurt, F. F. Muhammadsharif, H. N. Awl, S. Huang, and H. Luo, "The detection of chemical materials with a metamaterial-based sensor incorporating oval wing resonators," *Electronics*, Vol. 9, No. 5, May 2020.

[36] Mekki, S., R. Zegadi, S. Mosbah, D. Sayad, I. Elfergani, M. L. Bouknia, J. Rodriguez, A. Desai, M. Palandoken, and C. Zebiri, "Equivalent circuit of a planar microwave liquid sensor based on metamaterial complementary split ring resonator," *Frequenz*, Oct. 2023.

[37] Ghahremani, M., C. Ghobadi, J. Nourinia, M. S. Ellis, F. Alizadeh, and B. Mohammadi, "Miniaturised UWB antenna with dual-band rejection of WLAN/WIMAX using slitted EBG structure," *IET Microwaves Antennas & Propagation*, Vol. 13, No. 3, 360–366, Feb. 2019.

[38] Taha Ahmed, B. and D. B. Hernandez, "UWB fractal antennas with low group delay variation," *Wireless Personal Communications*, Vol. 114, No. 3, 1999–2016, Oct. 2020.